scientific reports

Check for updates

OPEN

# Soret and Dufour influences on forced convection of Cross radiative nanofluid flowing via a thin movable needle

M. Israr Ur Rehman[1], Haibo Chen[1], Aamir Hamid[2], Sajid Qayyum[3], Wasim Jamshed[4]✉, Zehba Raizah[5], Mohamed R. Eid[6,7] & El Sayed M. Tag El Din[8]

**The main feature of the current investigation is to analyze the magnetohydrodynamic mixed convection flow of Cross fluid. Flow is due to a movable thin needle with Soret and Dufour effect. Heat generation/absorption and nonlinear heat radiation are used in the energy equation. Characteristics of the chemical reaction and thermal activation are given special attention. Appropriate variables are introduced for the transformation of partial differential equations to ordinary differential equations. With the assistance of Runge–Kutta Fehlberg's fourth- fifth-order method with the shooting technique, we determined the prominent result numerically. The prominent examined parameters range is velocity and temperature ratios, heat generation, Dufour, Hartmann, Schmidt numbers ($0.1 \leq \lambda, \theta_w, Q, D_u, M, Sc \leq 0.7$), needle thickness ($0 \leq a \leq 15$), radiative parameter ($5 \leq Rd \leq 8$), and Weissenberg number ($0.01 \leq We \leq 0.09$), respectively. Graphs for velocity, thermal, concentration, Skin friction coefficient, and heat and mass transport rates are displayed and analyzed for physical parameters. A similar observation of mixed convection and needle thickness parameter is seen on the velocity field. Temperature and heat transfer rate are reverse behavior in the frame of the Dufour effect. Moreover, an enhancement in chemical reaction shows decay to the concentration field.**

**List of symbols**

| | |
|---|---|
| $u, v$ | Velocity components (m/s) |
| $x, y$ | Cartesian coordinates (m) |
| $n$ | Power law index |
| $T$ | Fluid temperature (K) |
| $Q$ | Heat generation parameter |
| $\rho_p$ | Density of nanoparticle |
| $T_w$ | Surface temperature (K) |
| Re | Local Reynolds number |
| $\mu$ | Generalized Newtonian viscosity (Pa s) |
| $\sigma$ | Electric conductivity |
| $U_w$ | Stretching velocity (m/s) |
| $k$ | Thermal conductivity (W/m K) |
| $B_0$ | Magnetic parameter |
| $\psi$ | Stream function |
| $\lambda_1$ | Mixed convection parameter |
| $C$ | Fluid concentration (kg/m$^3$) |
| $a$ | Needle thickness parameter |

[1]School of Mathematics and Statistics, Central South University, Changsha 410083, China. [2]Department of Mathematics, Women University of Azad Jammu and Kashmir, Bagh 12500, Azad Kashmir, Pakistan. [3]Department of Mathematics, University of Mianwali, Mianwali, Pakistan. [4]Department of Mathematics, Capital University of Science and Technology (CUST), Islamabad 44000, Pakistan. [5]Department of Mathematics, College of Science, King Khalid University, Abha, Saudi Arabia. [6]Department of Mathematics, Faculty of Science, New Valley University, Al-Kharga 72511, Al-Wadi Al-Gadid, Egypt. [7]Department of Mathematics, Faculty of Science, Northern Border University, Arar 1321, Saudi Arabia. [8]Electrical Engineering, Faculty of Engineering and Technology, Future University in Egypt, New Cairo 11835, Egypt. ✉email: wasiktk@hotmail.com

| | |
|---|---|
| $C_w$ | Surface volume fraction (kg/m$^3$) |
| $We$ | Local Weissenberg number |
| $T_\infty$ | Ambient temperature (K) |
| $D_u$ | Dufour number |
| $C_s$ | Concentration susceptibility |
| Pr | Prandtl number |
| $\phi$ | Dimensionless concentration |
| $Nu$ | Local Nusselt number |
| $\theta_w$ | Temperature ratio parameter |
| $K_r^2$ | Chemical reaction constant |
| $Sr$ | Soret number |
| $C_f$ | Skin friction coefficient |
| $\lambda$ | Velocity ratio parameter |
| $C_\infty$ | Ambient nanoparticle volume fraction (kg/m$^3$) |
| $M$ | Magnetic effect (kg/As$^2$) Tesla |
| $\nu_f$ | Kinematic viscosity (m$^2$/s) |
| $Rd$ | Radiation parameter |
| $g$ | Thermal expansion coefficient |
| $\theta$ | Dimensionless temperature |
| $\Gamma$ | Chemical reaction parameter |
| $\eta$ | Dimensionless similarity variable |
| $Sc$ | Schmidt number |
| $Nr$ | Buoyancy ratio parameter |
| $D_m$ | Mass diffusivity |
| $E$ | Activation energy |
| $C_p$ | Heat capacity |
| $\rho$ | Density of fluid (kg/m$^3$) |

Viscosities of the numerous liquids we come across every day are affected by the applying shear force. Although, there is various type of liquid that exhibits fundamentally different performance. Several of these fluids are shear-thicker, which means that the relation between their viscosities and the strain rate is inverse. Such application is exhibited in almost all mayonnaise, colloidal suspensions, polymer melts and solution, biological liquids, etc. A simplified two-effect (power-law) scheme, introduced by Oustwald[1] and well clarified by Reiner[2] has gained comprehensive discussion in the research for inelastic non-Newtonian liquids. This framework offers the shear rate curve and shear stress for a limited variety of shear rates. Munzar et al.[3] present an investigation of heat radiative and convective boundary condition impacts on a mixed convection thermal transport for the passage Cross liquid along a vertical stretched sheet into consideration of buoyancy impacts. Tochi[4] deduced analytic formulas connecting volumetric stream rate to pressured decline in circular tubes utilizing both the Cross-Carreau liquid schemes. The boundary layer computations for 2-dimensional stream and Cross-liquid energy transport passing through the linear stretched sheet were provided by Khan et al.[5]. Their research's conclusion depicts that enhancing the power-law effect the thicknesses of the heated boundary layer. Khan et al.[6] investigated a liquid stream around a radial extending disc embedded in a resting fluid satisfying a Cross-fluid scheme utilizing a computational method. Additionally, the most impressive current works are displayed in[7–10].

Flow across a thin needle has piqued the attention of investigators who expected its use in industrial products such as electrical devices, hot wire anemometers, and geothermal power generation. The thinner needle is identified as a body of change with a thickness smaller than that of the boundary layer. Lee[11] was the first to explore the flow of viscous liquid toward a thinner needle. The researchers next investigated this work by taking into consideration numerous physical aspects[12–15]. Mabood et al.[16] assessed the thermal management of the Cross-micropolar fluids stream over a thinner needle focusing on Arrhenius activation thermal and binary chemical reaction. Khan et al.[17] studied the heat transport for the stream of nanoliquid toward a thinner hot needle with the impacts of Hall current and viscous dissipation. Xiong et al.[18] examined the 2-dimensional, steady, laminar, and incompressible magneto-Cross nanoliquid flow across a movable vertical thinner needle with the incidence of chemical reaction, Darcy–Forchheimer permeable media, mixed convection, Ohmic, and viscous dissipation.

When thermal and mass transport appears concurrently in a changing liquid, the relationships between the fluxes and drive potentials become increasingly complex. It has been revealed that thermal fluxes may be produced not only by thermal estimation but also by concentric estimation. The diffusion-thermos (Dufour) effect describes heat transmission initiated by a concentric gradient. The mass transport produced by a temperature distribution, on the other hand, is known as the thermal-diffusive (Soret) influence. Such impacts are significant in hydrology, nuclear waste management, petrology, geothermal energy, nuclear reactors, oil reservoirs, groundwater pollutant migration, manufacture of rubber and plastic sheets, isotopes separation, the mixture of gases, and compact heat insulation exchangers. The consequences of the Dufour and Soret influences amalgamated with the Hartmann field on a Casson fluid across a stretchable surface are addressed by Hayat et al.[19]. Hayat et al.[20] explored the influences of, Soret and Dufour parameters on 3-dimensional second-grade MHD liquid stream through an exponentially radiative stretchable surface. Farooq et al.[21] investigated the incompressible electrically conducting Oldroyd-B liquid flow through a stretchable surface in the existence of Dufour and Soret impacts. Shojaei et al.[22] analytically assessed the stream of non-Newtonian liquid stream through a cylinder subjected to the thermal radiations, Soret, and Dufour consequences. Waini et al.[23] demonstrated the influences of Soret and Dufour and diffusive on the flow of $Al_2O_3$-water nanoliquid along a thinner needle by considering the Tiwari-Das

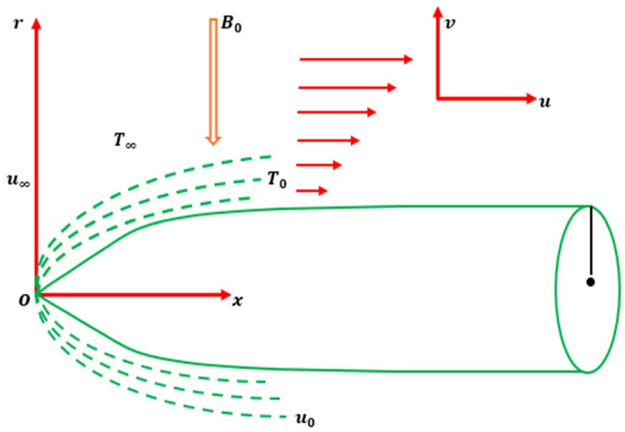


**Figure 1.** Flow geometry.

model. Rasool et al.[24] studied the outcomes of thermal radiation, chemical reaction, and Soret–Dufour influences on an incompressible steady Darcy–Forchheimer nanofluids flow along a stretchable surface. Alzahrani et al.[25] examined 3-dimensional, magnetohydrodynamic (MHD) embraced flow in a permeable rotating channel subject to viscous dissipation, applied magnetic field, Dufour and Soret impacts.

The minimal amount of energy needed to start a chemical reaction is identified as thermal activation. This concept of activation energy was first announced by Svante Arrhenius in the year 1889. In free convection boundary layer flows, thermal activation along with mass and heat transport has a considerable role. Thermal activation is particularly imperative in the sectors of the oil reservoir, mechanic chemistry, water emulsions, chemical engineering, geothermal industrial, and food management. Numerous researchers investigated the performance of activation energy in different media: Hayat et al.[26] studied Ree–Eyring nanoliquid flow with Arrhenius activation energy and entropy optimization between two rotating surfaces. Kalaivanan et al.[27] analyzed the influences of thermal activation on flow heat and mass transport features of second-grade nanoliquid over a stretching surface. Muhammad et al.[28] investigated the flow of Eyring–Powell nanoliquid with the consideration of modified thermal and mass fluxes, nonlinear heat radiative, velocity slip condition, and Arrhenius activation energy. Several recent attempts regarding activation energy can be seen through studies[29–40].

The peculiarity of this research is that it investigates the Cross-diffusion influence on the mixed convection stream of magnetized Cross liquid toward a vertical movable thin needle with Soret and Dufour variation. The governing system of flow mechanism is transformed into ordinary differential equations employing similarity transmission and then solved numerically by Runge–Kutta Fehlberg's fourth- fifth-order technique with a shooting scheme. The projections of developing parameters on drag coefficient, heat flux, and Sherwood numbers, with movement, thermal, and concentric curve are revealed in graphs and debated.

## Mathematical formulation

In this analysis, in the occurrence of Soret and Dufour variation, we examined an incompressible laminar boundary layer stream of a Cross nanoliquid across a movable thinner needle. Figure 1 shows a schematic illustration of the prominent scheme and coordinate system.

The axial and radial coordinates are $x$ and $r$, respectively, while the radius of the needle is $r = R(x)$. The needle leading edge is measured vertically on the $x$-axis, while $r$ is always perpendicular to the x-axis. The influence of the needle's transverse curvature is essential since it is thin, but the pressure gradient toward the surface can be ignored. We supposed that the needle surface thermal is $T_w$, with $T_w > \mathrm{T}$ indicating a heated needle (aiding flow) and $T_w < \mathrm{T}$ indicates a cooled needle (opposed flow), and that the surface volume fraction is $C_w > C$. Owing to the minimum magnetic Reynolds number, the Hartmann field $B_0$ is utilized parallel to the flow direction, and the generated Hartmann field can be neglected. The needle's movable constant velocity $U_w$, in a similar or opposing direction as a constant velocity U free stream flow. Additionally analyzed that the needle's size is thinner so that the pressure gradient is negligible while transverse curvature has a certain impact. The boundary layer description for mass, momentum, heat energy and solid volume fraction can be stated as follows under the preceding assumptions[13,17,41]:

$$\frac{\partial}{\partial x}(ru) + \frac{\partial}{\partial r}(rv) = 0 \tag{1}$$

$$\left.\begin{aligned} u\frac{\partial u}{\partial x} + v\frac{\partial u}{\partial r} = \nu_f\left(\frac{\partial}{\partial r} + \frac{1}{r}\right)\left[\left(\frac{\partial u}{\partial r}\right)\left\{1 + \left(\Gamma\left|\frac{\partial u}{\partial r}\right|^n\right)\right\}\right] - \frac{\sigma B_0^2 u}{\rho} \\ + \frac{1}{\rho_f}\left[(1 - C_\infty)\rho_{f\infty} B_T (T - T_\infty) - \left(\rho_p - \rho_{f\infty}\right)(C - C_\infty)\right] g \end{aligned}\right\} \tag{2}$$

$$u\frac{\partial T}{\partial x}+v\frac{\partial T}{\partial r}=\frac{K}{\rho_f C_p}\frac{1}{r}\frac{\partial}{\partial r}\left[\left(1+\frac{16\sigma_s}{3k_e k_f}T_\infty^3\right)\left(r\frac{\partial T}{\partial r}\right)\right]+\frac{D_m K_T}{cs}\frac{1}{r}(rC_r)_r \tag{3}$$

$$u\frac{\partial C}{\partial x}+v\frac{\partial C}{\partial r}=\frac{D}{r}\frac{\partial}{\partial r}\left(r\frac{\partial C}{\partial r}\right)+\frac{D_m K_T}{T_m}\frac{1}{r}(rT_r)_r-K_r^2(C-C_\infty)\left(\frac{T}{T_\infty}\right)^n e^{\frac{E_0}{K^*T}} \tag{4}$$

The associated boundary condition is[16]:

$$\begin{aligned} &u=U_w, v=0, T=T_w, C=C_w, r=R(x),\\ &u\to U_\infty, T\to T_\infty, C\to C_\infty, asr\to\infty \end{aligned} \tag{5}$$

where $u, v, T, n, \rho_f, T_\infty, C, \rho_p, \sigma, \nu_f, C_\infty, \mu, C_p, D_m, g, C_s, K_r^2$ and $Kr$ represents radial and axial velocity components, temperature, power law index, the density of fluid, ambient temperature, concentration, the density of nanoparticles, electric conductivity, kinematics viscosity, ambient concentration, dynamic viscosity, heat capacity, mass diffusivity, thermal expansion coefficient, concentration susceptibility, chemical reaction constant and chemical response parameter respectively.

## Nondimensional solve

The similarity transmission is[16]:

$$\eta=\frac{U_0 r^2}{\nu_f x}, \psi=\nu_f x f(\eta), \theta(\eta)=\frac{T-T_\infty}{T_w-T_\infty}, \phi(\eta)=\frac{C-C_\infty}{C_w-C_\infty} \tag{6}$$

where Eq. (1) is assured identically, and Eqs. (2–5) are interpreted into

$$R_e\left[1+(1-n)\left(4Wef''\right)^n\right]f'''+\frac{1}{2}\left[1+\left(4Wef''\right)^n\right]^2+ff''-Mf'+\frac{\lambda_1}{4}\theta-\frac{Nr}{4}\phi=0 \tag{7}$$

$$\frac{1}{Pr\left[\left(1+Rd(1+(\theta_w-1)\theta)^3\right)(\eta\theta')\right]'\frac{1}{2}\frac{D_u}{2}(\eta\phi''+\phi')} \tag{8}$$

$$2\eta\phi''+2\phi'+ScSr\left(\eta\theta''+\theta'\right)+\frac{Sc}{2}f\phi'-\frac{1}{2}\Gamma Sc\phi(1+\delta\theta)^n exp\left(\frac{-E}{1+\delta\theta}\right)=0 \tag{9}$$

$$\begin{aligned} &f(a)=\frac{\lambda}{2}a, \theta(a)=1, f'(a)=\frac{\lambda}{2}, \phi(a)=1,\\ &\theta(\eta)\to 0, f'(\eta)\to\left(\frac{1-\lambda}{2}\right), \phi(\eta)\to 0\ at\ \eta\to\infty \end{aligned} \tag{10}$$

where the dimensionless number in Eqs. (7–10) are $Re$, $\lambda_1$, $Pr$, $We$, $D_u$, $Rd$, $a$, $M$, $Nr$, $Sc$, $E$, $\theta_w$, $\Gamma$, $\lambda$, and $Sr$ represent Reynolds number, mixed convection factor, Prandtl number, Weissenberg number, Dufour number, radiation parameter, needle thickness variable, Hartmann number, buoyance ratio parameter, Schmidt number, activation energy parameter, temperature ratio parameter, chemical reaction parameter, heat generation/absorption variable, velocity ratio parameter, and Soret number via, are express below.

$$\left.\begin{aligned} We=\frac{u_w R_e}{U}, \lambda=\frac{Gr_x}{R_e}, Gr_x=\frac{(1-C_\infty)(T_w-T_\infty)gB_T}{\nu^2}, M=\frac{\sigma B_0^2 x}{2\rho U},\\ Nr=\frac{(\rho_p-\rho_{f\infty})C_\infty gx}{U^2\rho_f}, Pr=\frac{\rho C_p\nu}{K}, Rd=\frac{16\sigma_s T_\infty^3}{3k_e k_f}, Q=\frac{Q_0 x}{\rho C_p U},\\ Sc=\frac{\nu_f}{D}, \theta_w=\frac{T_w}{T_\infty}, Sr=\frac{(T_w-T_\infty)D_m K_T}{(C_w-C_\infty)T_m\mu C_p}, \Gamma=\frac{xK_r^2}{U}, \lambda=\frac{U_w}{U},\\ R_e=\frac{u_x}{\nu}, \delta=\frac{T_w-T_\infty}{T_\infty}, D_u=\frac{(C_w-C_\infty)D_m K_T}{(T_w-T_\infty)(cs\mu C_p)}, E=\frac{E_0}{KT_\infty} \end{aligned}\right\} \tag{11}$$

Here $C_{fx}$, $Nu_x$ and $Sh_x$ denotes friction factor coefficient, heat flux, and mass flux correspondingly.

$$\left.\begin{aligned} C_f=\frac{2\mu}{\rho U_w^2}\left\{1+\left(\Gamma\left|\frac{\partial u}{\partial r}\right|\right)^n\right\}^{-1}\left(\frac{\partial u}{\partial r}\right)_{r=R},\\ Nu_x=\frac{x}{K(T_w-T_\infty)}\left(\frac{\partial T}{\partial r}\right)_{r=R}+qr,\\ Sh_x=\frac{-x}{(C_w-C_\infty)}\left(\frac{\partial C}{\partial r}\right)_{r=R} \end{aligned}\right\} \tag{12}$$

In dimensionless form:

$$\left.\begin{aligned} f_x^{\frac{1}{2}}\left[\frac{f''(a)}{(1+We|f'''(a)|^n)}\right]\sqrt{Re}\\ Nu_x\mathrm{Re}_x^{-1/2}=-2a^{\frac{1}{2}}\left(1+Rd(1+(\theta_w-1)\theta(a))^3\right)\theta'(a),\\ Sh_x\mathrm{Re}_x^{-1/2}=-2a^{\frac{1}{2}}\phi'(a) \end{aligned}\right\} \tag{13}$$

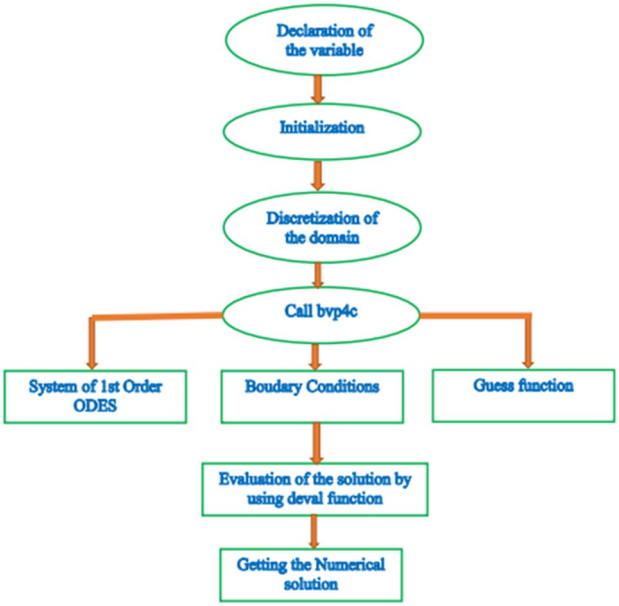


**Figure 2.** The flow chart of the numerical procedure.

where $Re_x = \frac{u_w}{\nu_f} x$ depicts the local Reynolds number.

## Numerical procedure

Due to the difficulty of obtaining an analytic solution for higher-order nonlinear ODEs, a suitable numerical technique with great convergence exactness must be adopted for this system. The numerical findings are obtained by RK-fourth order and shooting techniques.

Equations (1)–(4) along with Eq. (5) are solved with the combination of RK-fourth order and shooting techniques.

By utilizing $h_1 = f, h_2 = f', h_3 = f'', h_4 = \theta, h_5 = \theta', h_6 = \phi, h_7 = \phi'$

Equations (7)–(10) can be analyzed as per the rules:

$$\left.\begin{aligned}
h_1 &= h_2,\\
h_2 &= h_3,\\
h_3 &= \tfrac{1}{\mathrm{Re}[1+(1-n)(4We h_2)^n]}\left[\tfrac{1}{2}[1+(4We h_2)^n]^2 + h_1 h_2 + \tfrac{\lambda_1}{4} h_4 - \tfrac{Nr}{4} h_6\right],\\
h_4 &= h_5,\\
h_5 &= -\tfrac{\mathrm{Pr}}{(1+Rd(1+(\theta_w-1)h_4)^3)}\left[\begin{array}{c}\tfrac{1}{\mathrm{Pr}}\left[3\eta Rd(\theta_w-1)(1+(\theta_w-1)h_4)^2 h_5\right] + h_1 h_5\\ +\tfrac{1}{2}Q h_4 + \tfrac{D_u}{2}(\eta h_7 + h_7)\end{array}\right]\\
h_6 &= h_7,\\
h_7 &= -\tfrac{1}{2\eta}\left[2h_7 + ScSr(\eta h_5 + h_5) + \tfrac{Sc}{2} h_1 h_7 - \tfrac{1}{2}\Gamma Sch_6(1+\delta h_4)^n \exp\left(\tfrac{-E}{1+\delta h_4}\right)\right],
\end{aligned}\right\} \tag{14}$$

with

$$\left.\begin{aligned}
h_1(a) = \tfrac{\lambda}{2} a, h_4(a) = 1, h_2(a) = \tfrac{\lambda}{2}, h_6(0) = 1,\\
h_2(\infty) \to \left(\tfrac{1-\lambda}{2}\right), h_4(\infty) \to 0, h_6(\infty) \to 0.
\end{aligned}\right\} \tag{15}$$

In this development, the existence of a continuous outcome stimulates the grid choice and error function. The margin remains fixed at $10^{-4}$. The valuation of $\eta \to \infty$ implies that under this approach, each number response reaches asymptotic characteristics perfectly. The detailed flow chart has also been provided for a clearer and better comprehension of the existing shooting technique (see Fig. 2).

## Code validity

Table 1 is analyzed the comparison of the skin friction coefficient with the previously published article. It is observed that the present work is in good agreement with the preceding result in the limiting sense.

## Results and discussion

The present explanation illustrated the properties of comparative evaluation, velocity curve, heat flux, thermal field, mass flux, concentration estimation, and drag coefficient utilizing graphically and computed numerically. Figure 3a,b reveals the characteristics of the velocity curve $f'(\eta)$ for various needle thickness parameter ($a$) and velocity ratio parameter ($\lambda$). It is well known that improving ($a$) and ($\lambda$) decline the velocity curve $f'(\eta)$

| $M$ | Ref.[42] | Present |
|---|---|---|
| 0.0 | − 1.17372 | − 1.17365 |
| 0.2 | – | − 1.19004 |
| 0.4 | – | − 1.23805 |
| 0.6 | – | − 1.31454 |
| 0.8 | – | − 1.41526 |
| 10 | − 1.53571 | − 1.53570 |

**Table 1.** Comparison of $f''(0)$ with Makinde et al.[42] for numerous valuations of $M$ when $n = We = Nr = Re = \lambda_1 = 0$.

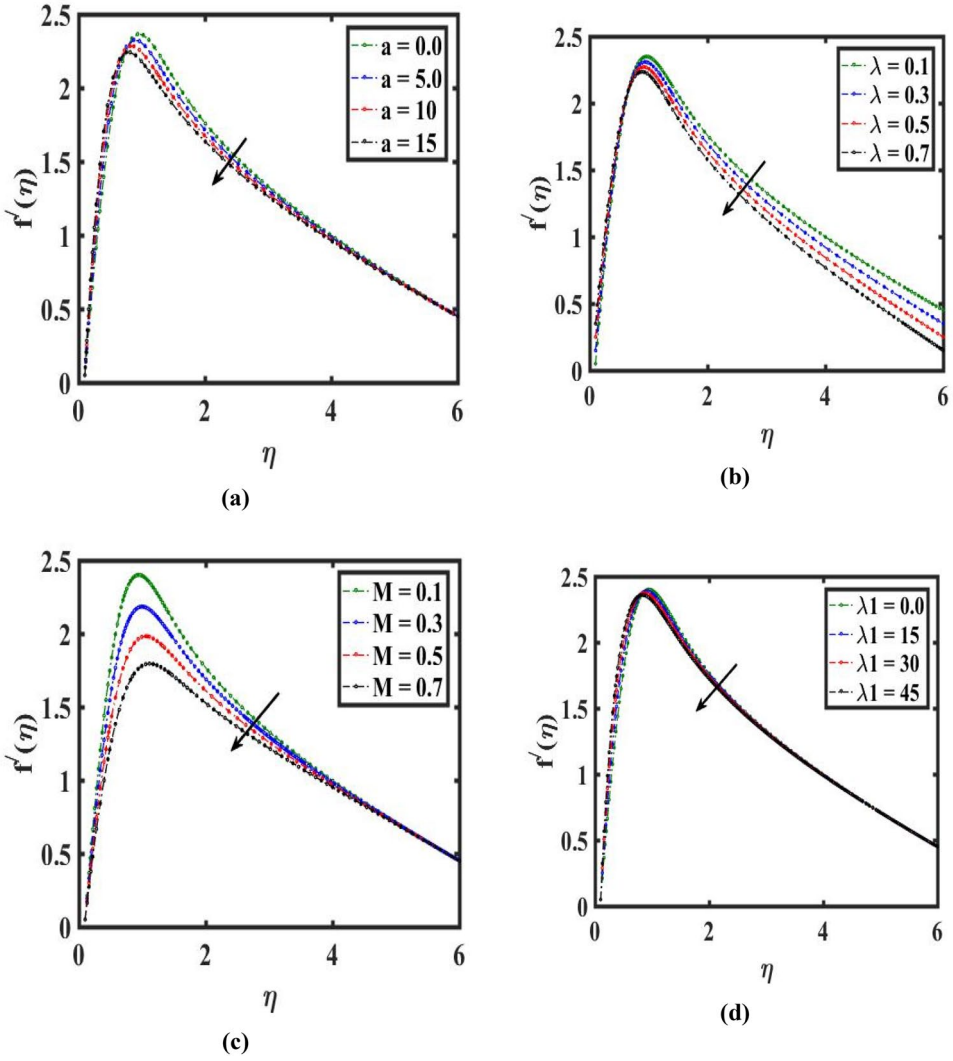


**Figure 3.** Variation of needle thickness $a$, velocity ratio $\lambda$, Hartmann number $M$, and mixed convection $\lambda_1$ on velocity $f'(\eta)$.

and momentum of liquid. Infect for a higher valuation of the thinner needle parameter the area of the needle is increase-es so the contact needle surface area with fluid increases which produces higher resistance to the liquid motion. Therefore, the velocity profile decreases. Figure 3c illustrates the stream controlling of the $(M)$ on the $f'(\eta)$. In this case, improving $(M)$ decays the momentum and velocity of the liquid. Actuality, it has been viewed that the presence of the Hartmann field in the flowing field area declines the liquid movement. This analysis demonstrated that the Hartmann force adds struggle to the flow which lowers its velocity. Figures 3d, 4a are presented to demonstrate the impact of $(\lambda_1)$ and $(Nr)$. It should be noticed that has been dropped in order

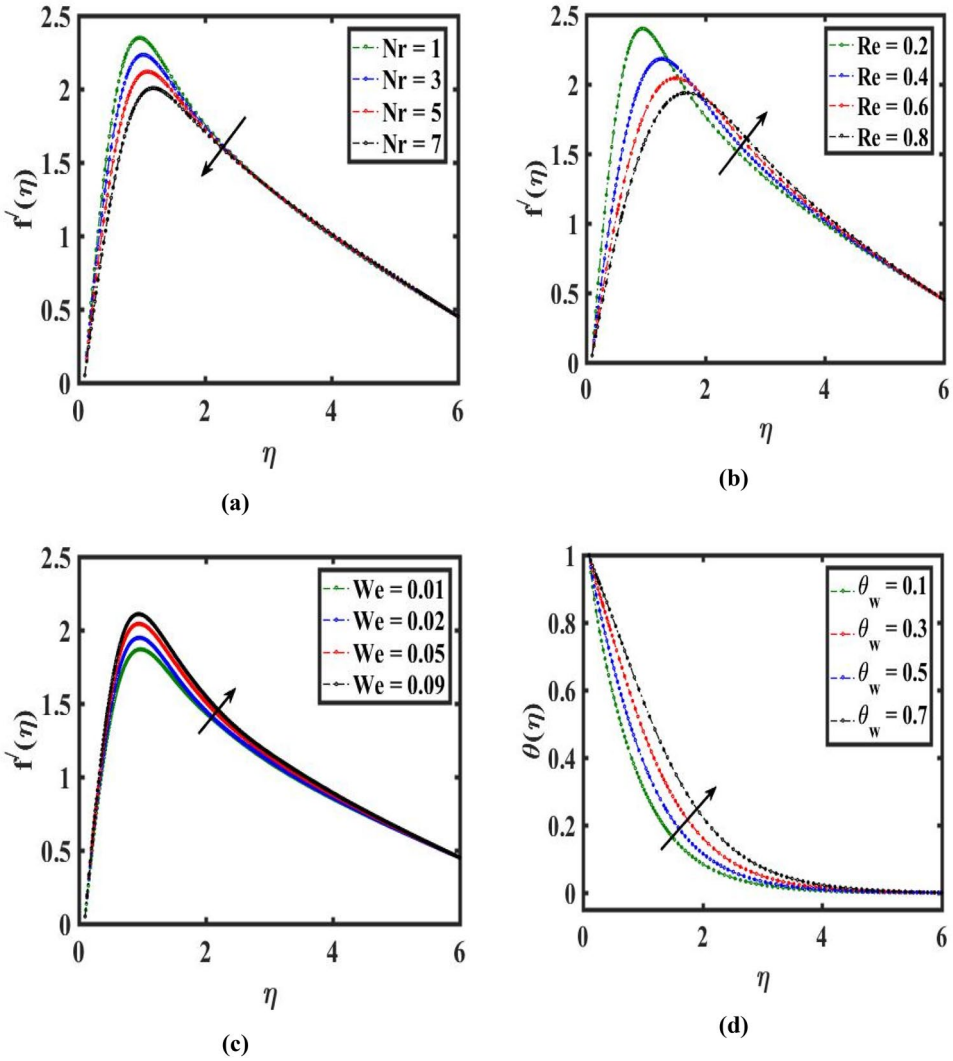


**Figure 4.** Impact of buoyance ratio $Nr$, Reynolds number $Re$, Weissenberg number $We$, and temperature ratio $\theta_w$ on velocity $f'(\eta)$ and temperature $\theta(\eta)$.

to improve the amount of $(\lambda_1)$. In addition, the $(\lambda_1)$ is associated with buoyance forces that restrict the liquid velocity from growing. As an outcome, for greater $(\lambda_1)$ liquid velocity drops. It is also discovered that the velocity curve diminishes by changing the estimation of $(Nr)$. The influence of $(R_e)$ and $(We)$ on the movement of liquid molecules are depicted in Fig. 4b,c. liquid velocity and associated layer thicker raises are noticed for improving assessment of $(R_e)$. It is also demonstrated that with bigger estimates of $(We)$, velocity climbs. Pertinently, an increment in time of relaxing leads to an augmented in $f'(\eta)$.

The variance of $\theta(\eta)$ for distinct estimation of $(\theta_w)$ and $(D_u)$ is highlighted in Figs. 4d, 5a. we can deduce $\theta(\eta)$ from these figures that climb for growth $(\theta_w)$ but the reverse pattern can be observed for $(D_u)$. Basically, a greater scale of $(\theta_w)$ represent larger melting thermal as compared to ambient liquid thermal. As an outcome, $\theta(\eta)$ improves. On augmenting in $(D_u)$ thermal curve $\theta(\eta)$ decays which outcomes in heat transport. Thus, a physical improvement is investigated in the temperature estimation $\theta(\eta)$ which is very significant for the stretchable needle.

Figure 5b provides a variety of temperatures because of $(Pr)$. Since $(Pr)$ corelates between the momentum and thermal diffusivities. Here larger $(Pr)$ leads to low thermal diffusivity which shows decay temperature. Figure 5c displays the behavior of heat generating and absorbing variable $(Q)$ on $\theta(\eta)$. It is observed that when $(Q)$ is boosted, a large estimation of thermal is produced. As a result, the mechanisms of higher heat and hence the thermal curve $\theta(\eta)$ escalate. Figure 5d highlights the tendency of the boundary-layered stream field curve towards the variation in the amplitude of $(Rd)$. It is clear from the figure that has a greater influence of $(Rd)$ on thermal estimation $\theta(\eta)$. It is demonstrated that the thermal curve $\theta(\eta)$ is optimized as $(Rd)$ upsurges. This assumption supports the fact that $(Rd)$ is important for delivering additional heat in the liquid stream process.

The change of $\phi(\eta)$ through $(Sc)$ is represented in Fig. 6a. this graph noticed that $\phi(\eta)$ and its associated layer thicker are declines for climbs estimation of $(Sc)$. In addition, for raising the estimation of $(Sc)$. $\phi(\eta)$ feels decay

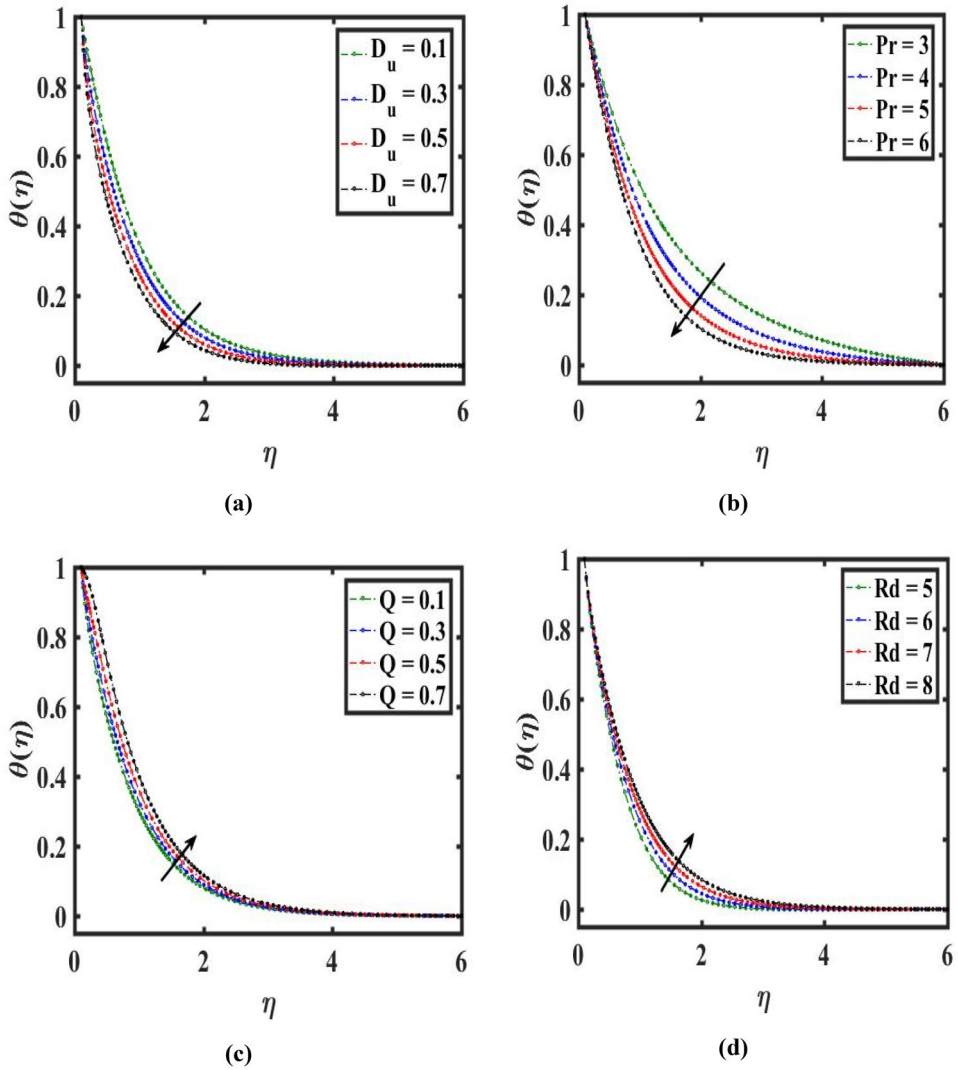


**Figure 5.** Effect of Dufour number $D_u$, Prandtl number $Pr$, heat generation $Q$ and radiation $Rd$ on temperature $\theta(\eta)$.

due to it. The variability of the concentric distribution $\phi(\eta)$ with $(\Gamma)$ is revealed in Fig. 6b. As the amount of $(\Gamma)$ climbs the concentric of species in the boundary layered falls. Figure 6c highlights the influence of the drag coefficient along $(M)$ and $(Nr)$. Here, augmenting estimation of $(M)$ decay the $f''(0)$. Figure 7a displays the friction factor coefficient change towards $(\lambda)$ and $(\lambda_1)$. Here, a higher amount of $(\lambda)$ diminishes the $f'\prime(0)$. The change in heat flux through $(Q)$ and $(Rd)$ is depicted in Fig. 7b. Here, $-\theta'(0)$ reduces for enhancing estimation of $(Q)$ and falls for improving the estimation of $(Rd)$. The variation in heat flux towards $(D_u)$ and $(Rd)$ is illustrated in Fig. 7c. Here, $-\theta'(0)$ acts as an escalating function of $(D_u)$ and diminishing function of $(Rd)$. The difference in mass flux through $(Sc)$ and $(\Gamma)$ is revealed in Fig. 7d. Here, $-\phi'(0)$ upsurge for escalating estimation of $(Sc)$ and decays for higher in the amount of $(\Gamma)$.

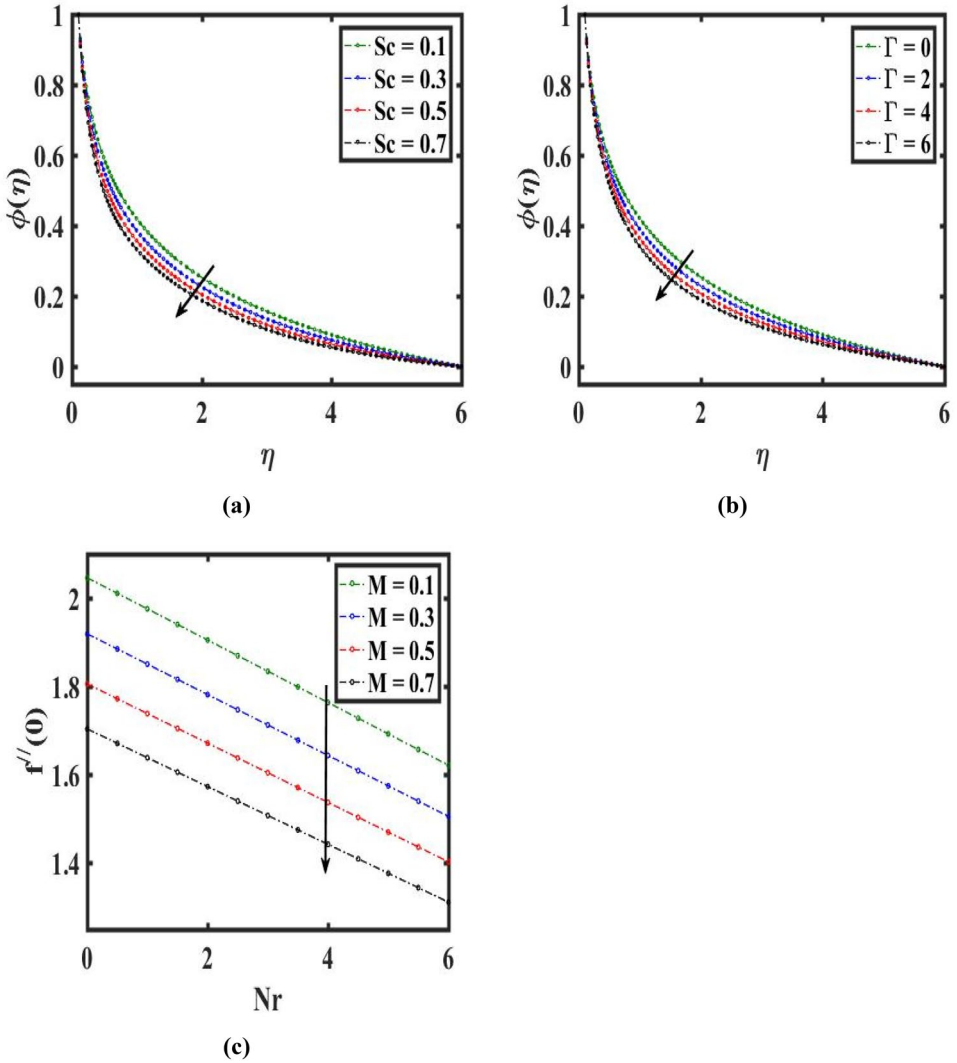


**Figure 6.** Effect of Schmidt number *Sc*, chemical reaction Γ, Hartmann number *M*, and buoyance ratio *Nr* on concentration $\phi(\eta)$ and velocity $f''(0)$.

## Concluding Remarks

A numerical study of the melting heat transport process in MHD flow of Cross fluid passing on a movable thinner needle is investigated. The influences of nonlinear heat radiative, Soret, and Dufour on mixed convection flow have been taken into consideration. Additional changes in the binary chemical reaction and thermal generation have also been studied. The core observations of the current study are summarized as follows:

- Large estimations of $\lambda_1$ and *Nr* yields the velocity field and thickness of the momentum boundary layer.
- Reverse behavior of the thermal field is analyzed in the frame of $D_u$ and *Rd*.
- Qualitative impact of concentration and Sherwood number are reversed when *Sc* is enhanced.
- Coefficient of Skin fraction is decay via mixed convection parameters.
- Local heat flux is improved because of the Dufour effect.
- Local mass flux is an increasing function of the Schmidt number.

The RK-fourth order and shooting techniques could be applied to a variety of physical and technical challenges in the future[43–50].

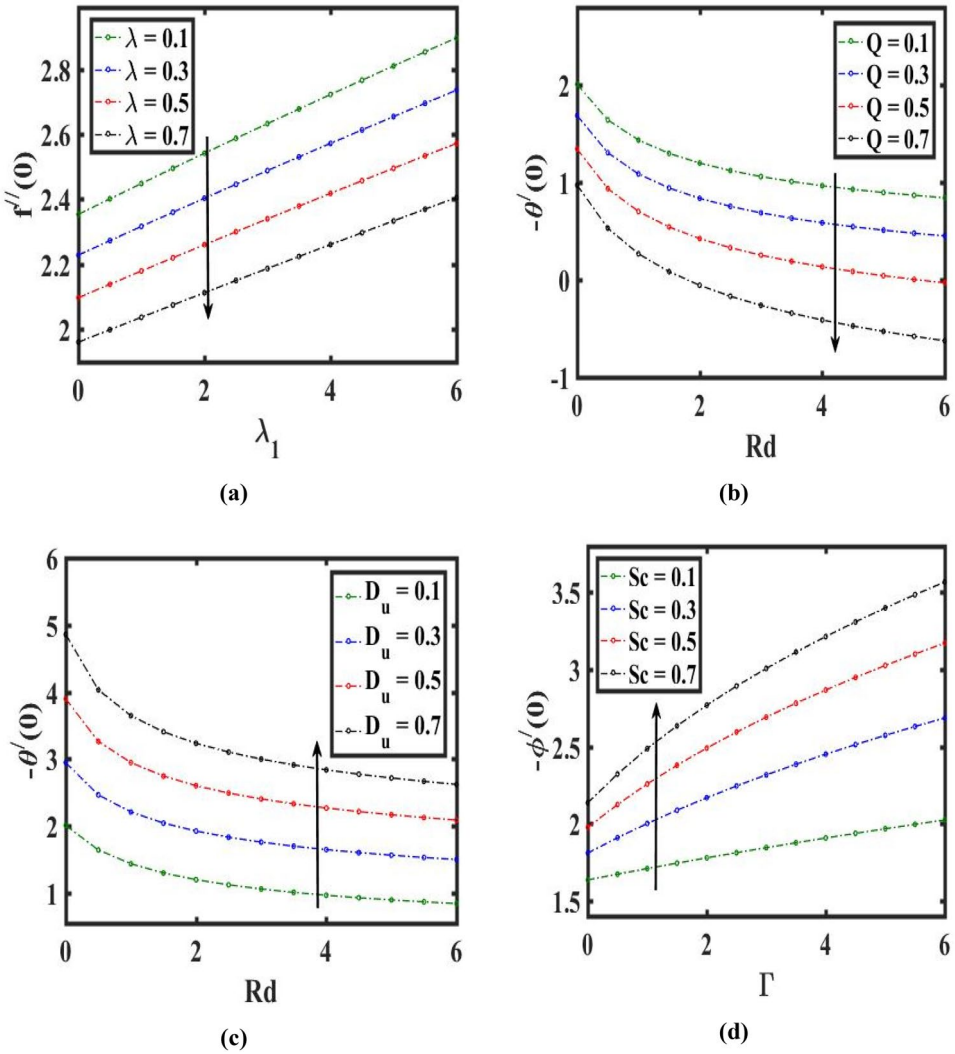


**Figure 7.** Influences of velocity ratio $\lambda$, mixed convection $\lambda_1$, heat generation $Q$, Dufour number $D_u$, radiation $Rd$, Schmidt number $Sc$ and chemical reaction $\Gamma$ on drag force $f''(0)$, heat transfer $-\theta'(0)$ and mass transfer $-\phi'(0)$.

## Date availability

All data generated or analyzed during this study are included in this published article.

Received: 21 August 2022; Accepted: 2 November 2022
Published online: 04 November 2022

## References

1. Ostwald, W. Ueber die rechnerische Darstellung des Strukturgebietes der Viskosität. *Kolloid-Zeitschrift* **47**(2), 176–187 (1929).
2. Reiner, M. & Schoenfeld-Reiner, R. Viskosimetrische Untersuchungen an Lösungen hochmolekularer Na-turstoffe. *I. Mitteilung. Kautschuk in Toluol. Kolloid-Zeitschrift* **65**(1), 44–62 (1933).
3. Manzur, M., Khan, M. & ur Rahman, M.,. Mixed convection heat transfer to cross fluid with thermal radiation: effects of buoyancy assisting and opposing flows. *Int. J. Mech. Sci.* **138**, 515–523 (2018).
4. Sochi, T. Analytical solutions for the flow of Carreau and Cross fluids in circular pipes and thin slits. *Rheol. Acta* **54**(8), 745–756 (2015).
5. Khan, M., & Manzur, M. Boundary layer flow and heat transfer of Cross fluid over a stretching sheet. arXiv preprint arXiv:1609.01855 (2016).
6. Khan, M., Manzur, M. & ur Rahman, M.,. On axisymmetric flow and heat transfer of Cross fluid over a radially stretching sheet. *Res. Phys.* **7**, 3767–3772 (2017).
7. Hauswirth, S. C. *et al.* Modeling cross model non-Newtonian fluid flow in porous media. *J. Contam. Hydrol.* **235**, 103708 (2020).
8. Hina, S., Shafique, A. & Mustafa, M. Numerical simulations of heat transfer around a circular cylinder im-mersed in a shear-thinning fluid obeying Cross model. *Phys. A* **540**, 123184 (2020).
9. Rehman, K. U., Awan, F. J., Qaiser, A. & Mehmood, A. On Joule heating magnetized axisymmetric Cross fluid model: A computational statistics. *Phys. A* **534**, 122134 (2019).
10. Hosseinzadeh, K. *et al.* Investigation of cross-fluid flow containing motile gyrotactic microorganisms and nanoparticles over a three-dimensional cylin-der. *Alex. Eng. J.* **59**(5), 3297–3307 (2020).

11. Lee, L. L. Boundary layer over a thin needle. *Phys. Fluids* **10**(4), 820–822 (1967).
12. Hayat, T., Khan, M. I., Farooq, M., Yasmeen, T. & Alsaedi, A. Water-carbon nanofluid flow with variable heat flux by a thin needle. *J. Mol. Liq.* **224**, 786–791 (2016).
13. Ahmad, R., Mustafa, M. & Hina, S. Buongiorno's model for fluid flow around a moving thin needle in a flowing nanofluid: A numerical study. *Chin. J. Phys.* **55**(4), 1264–1274 (2017).
14. Khan, M. W. A., Khan, M. I., Hayat, T. & Alsaedi, A. Entropy generation minimization (EGM) of nanofluid flow by a thin moving needle with nonlinear thermal radiation. *Phys. B* **534**, 113–119 (2018).
15. Waini, I., Ishak, A., & Pop, I. Hybrid nanofluid flow and heat transfer past a vertical thin needle with pre-scribed surface heat flux. *Int. J. Num. Methods Heat Fluid Flow* (2019).
16. Mabood, F., Nayak, M. K. & Chamkha, A. J. Heat transfer on the cross flow of micropolar fluids over a thin needle moving in a parallel stream influenced by binary chemical reaction and Arrhenius activation energy. *Eur. Phys. J. Plus* **134**(9), 427 (2019).
17. Khan, A. *et al.* Chemically reactive nanofluid flow past a thin moving needle with viscous dissipation, magnetic effects and hall current. *PLoS ONE* **16**(4), e0249264 (2021).
18. Xiong, P. Y. *et al.* Dynamics of multiple solutions of Darcy-Forchheimer saturated flow of Cross nanofluid by a vertical thin needle point. *Eur. Phys. J. Plus* **136**(3), 1–22 (2021).
19. Hayat, T., Shehzad, S. A. & Alsaedi, A. Soret and Dufour effects on magnetohydrodynamic (MHD) flow of Casson fluid. *Appl. Math. Mech.* **33**(10), 1301–1312 (2012).
20. Hayat, T., Ullah, I., Muhammad, T. & Alsaedi, A. Radiative three-dimensional flow with Soret and Dufour effects. *Int. J. Mech. Sci.* **133**, 829–837 (2017).
21. Farooq, A., Ali, R. & Benim, A. C. Soret and Dufour effects on three dimensional Oldroyd-B fluid. *Phys. A* **503**, 345–354 (2018).
22. Shojaei, A., Amiri, A. J., Ardahaie, S. S., Hosseinzadeh, K. & Ganji, D. D. Hydrothermal analysis of non-Newtonian second grade fluid flow on radiative stretching cylinder with Soret and Dufour effects. *Case Stud. Therm. Eng.* **13**, 100384 (2019).
23. Waini, I., Ishak, A., & Pop, I. Dufour and Soret effects on $Al_2O_3$-water nanofluid flow over a moving thin needle: Tiwari and Das model. *Int. J. Numer. Methods Heat Fluid Flow* (2020).
24. Rasool, G., Shafiq, A. & Baleanu, D. Consequences of Soret-Dufour effects, thermal radiation, and binary chemical reaction on Darcy Forchheimer flow of nanofluids. *Symmetry* **12**(9), 1421 (2020).
25. Alzahrani, A. K., Ullah, M. Z. & Muhammad, T. Numerical treatment for 3D squeezed flow in a rotating channel with Soret and Dufour effects. *Front. Phys.* **8**, 201 (2021).
26. Hayat, T., Khan, S. A., Khan, M. I. & Alsaedi, A. Theoretical investigation of Ree-Eyring nanofluid flow with entropy optimization and Arrhenius activation energy between two rotating disks. *Comput. Methods Programs Biomed.* **177**, 57–68 (2019).
27. Kalaivanan, R., Ganesh, N. V. & Al-Mdallal, Q. M. An investigation on Arrhenius activation energy of sec-ond grade nanofluid flow with active and passive control of nanomaterials. *Case Stud. Therm. Eng.* **22**, 100774 (2020).
28. Muhammad, T., Waqas, H., Khan, S. A., Ellahi, R. & Sait, S. M. Significance of nonlinear thermal radiation in 3D Eyring-Powell nanofluid flow with Arrhenius activation energy. *J. Therm. Anal. Calorim.* **143**(2), 929–944 (2021).
29. Bhatti, M. M. & Michaelides, E. E. Study of Arrhenius activation energy on the thermo-bioconvection nanofluid flow over a Riga plate. *J. Therm. Anal. Calorim.* **143**(3), 2029–2038 (2021).
30. Shaheen, N., Alshehri, H. M., Ramzan, M., Shah, Z. & Kumam, P. Soret and Dufour effects on a Casson nanofluid flow past a deformable cylinder with variable characteristics and Arrhenius activation energy. *Sci. Rep.* **11**(1), 1–19 (2021).
31. Saeed, A. & Gul, T. Bioconvection Casson nanofluid flow together with Darcy-Forchheimer due to a rotating disk with thermal radiation and Arrhenius activation energy. *SN Appl. Sci.* **3**(1), 1–19 (2021).
32. Maraj, E. N., Khatoon, Z., Ijaz, S. & Mehmood, R. Effect of arrhenius activation energy and medium porosity on mixed convective diluted ethylene glycol nanofluid flow towards a curved stretching surface. *Int. Commun. Heat Mass Transfer* **129**, 105691 (2021).
33. Ebrahimi, D. *et al.* Mixed convection heat transfer of a nanofluid in a closed elbow-shaped cavity (CESC). *J. Therm. Anal. Calorim.* **144**(6), 2295–2316 (2021).
34. Yousefzadeh, S. *et al.* Numerical investiga-tion of mixed convection heat transfer behavior of nanofluid in a cavity with different heat transfer areas. *J. Therm. Anal. Calorim.* **140**(6), 2779–2803 (2020).
35. Nazari, S. *et al.* Numerical study on mixed convection of a non-Newtonian nanofluid with porous media in a two lid-driven square cavity. *J. Therm. Anal. Calorimet.* **140**(3), 1121–1145 (2020).
36. Hajatzadeh Pordanjani, A., Aghakhani, S., Karimipour, A., Afrand, M. & Goodarzi, M. Investigation of free convection heat transfer and entropy generation of nanofluid flow inside a cavity affected by magnetic field and thermal radiation. *J. Therm. Anal. Calorim.* **137**(3), 997–1019 (2019).
37. Shafiq, A. *et al.* Thermally enhanced Darcy-Forchheimer Casson-water/glycerine rotating nanofluid flow with uniform magnetic field. *Micromachines* **12**(6), 605 (2021).
38. Rasool, G., Shafiq, A. & Durur, H. Darcy-Forchheimer relation in Magnetohydrodynamic Jeffrey nanofluid flow over stretching surface. *Disc. Contin. Dyn. Syst. S* **14**(7), 2497 (2021).
39. Ali, B., Hussain, S., Shafique, M., Habib, D. & Rasool, G. Analyzing the interaction of hybrid base liquid $C_2H_6O_2$–$H_2O$ with hybrid nano-material Ag–$MoS_2$ for unsteady rotational flow referred to an elongated surface using modified Buongiorno's model: FEM simulation. *Math. Comput. Simul.* **190**, 57–74 (2021).
40. Ali, B., Rasool, G., Hussain, S., Baleanu, D. & Bano, S. Finite element study of magnetohydrodynamics (MHD) and activation energy in Darcy-Forchheimer rotating flow of Casson Carreau nanofluid. *Processes* **8**(9), 1185 (2020).
41. Soid, S. K., Ishak, A. & Pop, I. Boundary layer flow past a continuously moving thin needle in a nanoflu-id. *Appl. Therm. Eng.* **114**, 58–64 (2017).
42. Makinde, O. D., Mabood, F., Khan, W. A. & Tshehla, M. S. MHD flow of a variable viscosity nanofluid over a radially stretching convective surface with radiative heat. *J. Mol. Liq.* **219**, 624–630 (2016).
43. Bhatti, M. M., Öztop, H. F., Ellahi, R., Sarris, I. E. & Doranehgard, M. H. Insight into the investigation of diamond (C) and Silica ($SiO_2$) nanoparticles suspended in water-based hybrid nanofluid with application in solar collector. *J. Mol. Liq.* **357**, 119134 (2022).
44. Shah, S. S., Öztop, H. F., Ul-Haq, R., & Abu-Hamdeh, N. Natural convection process endorsed in coaxial duct with Soret/Dufour effect. *Int. J. Numer. Methods Heat Fluid Flow* (2022) (ahead-of-print).
45. Fares, R., Mebarek-Oudina, F., Aissa, A., Bilal, S. M. & Öztop, H. F. Optimal entropy generation in Darcy-Forchheimer magnetized flow in a square enclosure filled with silver-based water nanoliquid. *J. Therm. Anal. Calorim.* **147**(2), 1571–1581 (2022).
46. Pasha, A. A. *et al.* Statistical analysis of viscous hybridized nanofluid flowing via Galerkin finite element technique. *Int. Commun. Heat Mass Transfer* **137**, 106244 (2022).
47. Akram, M. *et al.* Irregular heat source impact on Carreau nanofluid flowing via exponential expanding cylinder: A thermal case study. *Case Stud. Therm. Eng.* **36**, 102190 (2022).
48. Jamshed, W. *et al.* Entropy production simulation of second-grade magnetic nanomaterials flowing across an expanding surface with viscidness dissipative flux. *Nanotechnol. Rev.* **11**, 2814–2826 (2022).
49. Alkathiri, A. A. & Jamshed, W. Galerkin finite element inspection of thermal distribution of renewable solar energy in presence of binary nanofluid in parabolic trough solar collector. *Alex. Eng. J.* **61**, 11063–11076 (2022).
50. Islam, N., Pasha, A. A., Jamshed, W., Ibrahim, R. W. & Alsulami, R. On Powell–Eyring hybridity nanofluidic flow based carboxy-methyl-cellulose (CMC) with solar thermal radiation: A quadratic regression estimation. *Int. Commun. Heat Mass Transfer* **138**, 106413 (2022).

## Acknowledgements
The author (Z. Raizah) extend her appreciation to the Deanship of Scientific Research at King Khalid University, Abha, Saudi Arabia, for funding this work through the Research Group Project under Grant Number (RGP.1/334/43).

## Author contributions
Conceptualization: M.I.U.R. Formal analysis: H.C. Investigation: W.J. Methodology: A.H. Software: S.Q. and E.S.M.T.E.D. Re-graphical representation and adding analysis of data: M.R.E. Writing—original draft: W.J. and E.S.M.T.E.D. Writing—review editing: Z.R. Re-modelling design: Z.R. Re-validation: M.R.E. Furthermore, all the authors equally contributed to the writing and proofreading of the paper. All authors reviewed the manuscript.

## Competing interests
The authors declare no competing interests.

## Additional information
**Correspondence** and requests for materials should be addressed to W.J.

**Reprints and permissions information** is available at www.nature.com/reprints.

**Publisher's note** Springer Nature remains neutral with regard to jurisdictional claims in published maps and institutional affiliations.